NANO LETTERS

LETTER

pubs.acs.org/NanoLett

Electrical Transport Properties of Oligothiophene-Based Molecular Films Studied by Current Sensing Atomic Force Microscopy

Bas L. M. Hendriksen,[†,▽] Florent Martin,[†,‡] Yabing Qi,[†,○] Clayton Mauldin,[§] Nenad Vukmirovic,[†,◆] JunFeng Ren,[†,∥] Herbert Wormeester,[⊥] Allard J. Katan,[†] Virginia Altoe,[#] Shaul Aloni,[#] Jean M. J. Fréchet,[§] Lin-Wang Wang,[†] and Miquel Salmeron*[,†,‡]

[†]Materials Science Division, Lawrence Berkeley National Laboratory, Berkeley, California 94720, United States

[‡]Materials Science and Engineering Department, University of California Berkeley, Berkeley, California 94720, United States

[§]Department of Chemistry, University of California Berkeley, Berkeley, California 94720, United States

[∥]College of Physics and Electronics, Shandong Normal University, Jinan, 250014, China

[⊥]MESA+ Institute for Nanotochnology, Faculty of Science and Technology University of Twente, Enschede, The Netherlands

[#]The Molecular Foundry, Lawrence Berkeley National Laboratory, Berkeley, California 94720, United States

Supporting Information

ABSTRACT: Using conducting probe atomic force microscopy (CAFM) we have investigated the electrical conduction properties of monolayer films of a pentathiophene derivative on a SiO_2/Si-p+ substrate. By a combination of current−voltage spectroscopy and current imaging we show that lateral charge transport takes place in the plane of the monolayer via hole injection into the highest occupied molecular orbitals of the pentathiophene unit. Our CAFM data suggest that the conductivity is anisotropic relative to the crystalline directions of the molecular lattice.

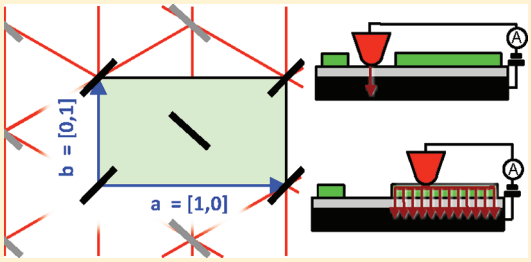

KEYWORDS: Oligothiophene, Langmuir−Blodgett monolayer, current sensing atomic force microscopy, molecular electronics, conduction anisotropy, lateral transport

The use of molecules as components of molecular scale electronic devices is a field of continuous interest, both in its fundamental scientific aspects and for potential applications in devices such as organic light emitting diodes and biosensors.[1−3] However, the electronic properties of the molecules and the correlation with their structure and assembly is still not well understood. Such understanding is necessary for the discovery of new properties and for the design of molecular scale devices. Efforts in that direction are underway in various laboratories. For example, intra- and intermolecular charge transport mechanisms have been studied in single molecules,[4] in molecular monolayers, in thin films,[5−8] in molecular crystals[9] and in biomolecular materials.[10]

Using conducting probe (current sensing) atomic force microscopy (CAFM) we investigated the electrical conduction properties of monolayer films of an oligothiophene derivative, 4-(5′′′′-Decyl-[2,2′;5′,2″;5″,2‴;5‴,2⁗] pentathiophen-5-yl)-butyric acid, or D5TBA for short (Figure 1a). Oligo- and poly thiophenes are p-type semiconductors that have applications in electronic devices and photovoltaics.[11,12] The structural and mechanical properties of self-assembled monolayers of D5TBA and of a similar molecule, TD5TBA on mica, have been studied previously with AFM.[13−15]

In this work, we show how electric charge is transported over micrometer distances away from the point of injection in monolayer thin films of oligothiophene molecules. The experimental setup that made this study possible is an unconventional diode configuration, where one electrode (the Si-p^+ substrate) is covered by a thin insulating SiO_2 film and the other electrode is a conductive Pt-coated tip of an AFM. The SiO_2 film plays a crucial role because it prevents the conducting substrate from short-circuiting the molecules, effectively separating conduction channels through and across the molecules (Figure 1g). The current flowing laterally through the oligothiophene molecules is determined from the increase in tip-to-substrate current. In other words, we do not measure the current between the AFM tip and a laterally separated electrode;[8,16] instead the lateral transport is determined from its contribution to the current flowing from the CAFM tip and spreading through the molecular film before going to the substrate. We use CAFM to simultaneously determine the structure and the charge transport properties. CAFM has the advantage of preserving the structural integrity of the film, whereas contacting the molecular monolayers with microfabricated electrodes generally disrupts the layers.

Structure of the D5TBA Monolayer. The molecular films of D5TBA were prepared using the Langmuir−Blodgett (LB) technique. The typical morphology of D5TBA on native-SiO_2/

Received: May 17, 2011
Revised: August 17, 2011
Published: August 17, 2011

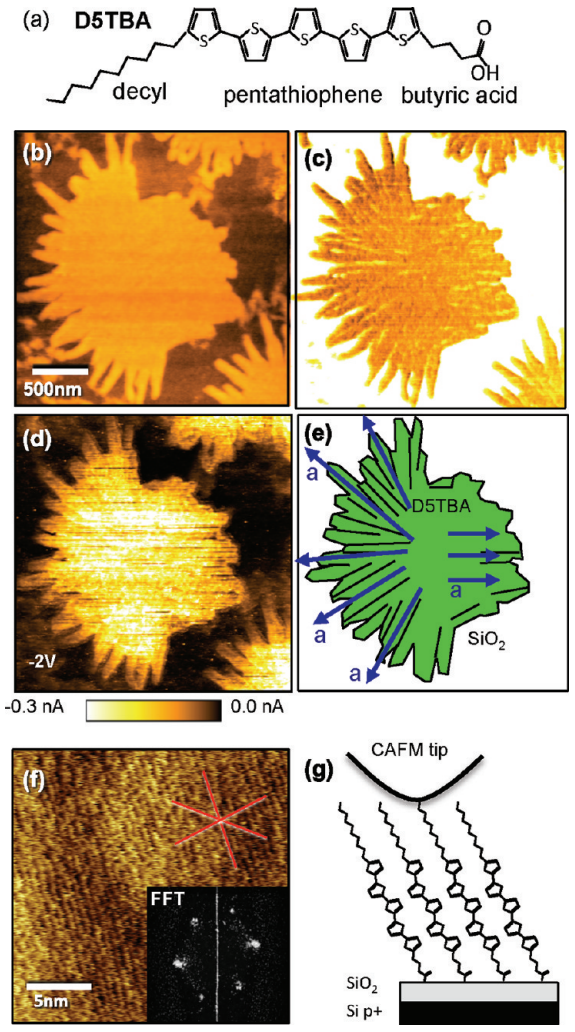

Figure 1. (a) Structure of the decyl-pentathiophene-butyric acid (D5TBA) molecule. (b) Topography of a characteristic monolayer island of D5TBA on SiO_2/Si. (c) Friction image, with dark corresponding to lower friction. (d) Image of the current measured at the tip at −2 V sample voltage. (e) Schematic representation of the D5TBA island. Black lines represent domain boundaries, blue arrows indicate the *a* direction of the molecular lattice (see Figure 2a). (f) Lattice-resolved friction image of one domain; red lines indicate the molecular lattice row directions in real space; the Fourier transform is shown in the inset. (g) Schematic of D5TBA molecules on a silicon substrate covered by the native oxide.

Si imaged by AFM is shown in Figure 1b,c. The film is always in the form of flowerlike islands with an island−island separation determined by the surface pressure during emersion of the sample from the LB trough. The height of the islands is 2.5 nm, which is smaller than 3.65 nm expected for fully extended molecules. The friction force on the islands is always lower than on the substrate (Figure 1c) due to the inert and lubricating properties of the exposed alkane chains. The size of the island varies from hundreds to thousands of nanometers. They are composed of elongated fingerlike domains extending roughly radially from the center as a result of nucleation from a point close to the center (Figure 1e). The domains are separated by boundaries that are particularly visible in friction images by the larger value of the force as the tip scans over them (Figure 1c).

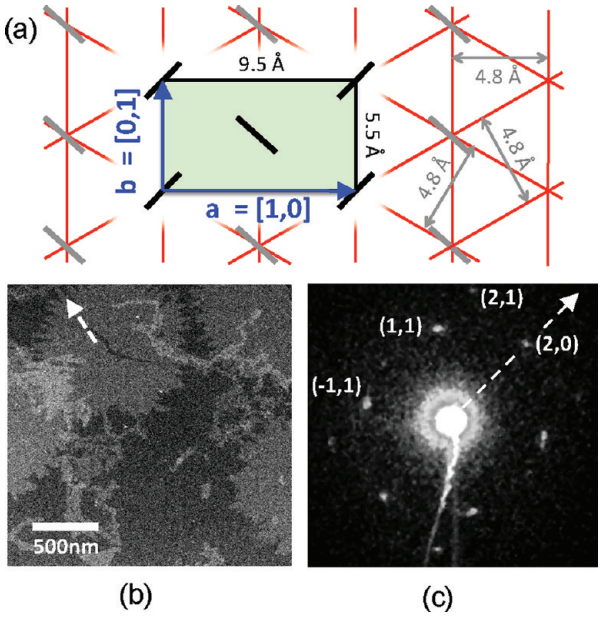

Figure 2. (a) Schematic top view of the Herringbone structure. Red lines represent directions where the molecules are most closely packed. These are the lattice rows resolved in the AFM images. Black and grey segments represent the thiophene units (b) TEM image of islands on a SiN substrate. The arrow indicates the *a* direction of the lattice in real space on the fingerlike domain where the diffraction pattern (c) was recorded. (c) TEM diffraction pattern. Notice the absence of (1,0) and (0,1) diffraction spots. The *a* direction in reciprocal space is shown by the arrow.

This is consistent with the general observation that structural disorder gives rise to higher friction.[17] The CAFM current image shown in Figure 1d was recorded simultaneously with Figure 1b,c and will be discussed below.

Figure 1f shows a lattice resolved AFM friction image from one domain of the D5TBA islands on the SiO_2/Si substrate. The Fourier transform of the image (inset in Figure 1f) shows a nearly hexagonal symmetry. We found that D5TBA films deposited on mica have the same morphology and structure as D5TBA on SiO_2/Si substrates. Lattice-resolved images of the mica substrate obtained in the same experiment were used as a reference to correct for image distortions due to thermal drift and nonlinearity of the piezo scanner. In this way, the spacing between rows of molecules was measured to be 4.8 ± 0.4 Å and the angle between lattice directions 60 ± 5°. Such an apparent hexagonal lattice is consistent with the well-known Herringbone structure commonly found for planar π-systems.[5]

In the AFM experiments, the AFM tip is in contact with the alkyl chains and the orientation of the thiophene rings is not visible. This and the fact that we measure similar row spacings of 4.8 Å for each direction prevents us from unambiguously indexing the lattice directions in the images. To obtain more information on the structure of the unit cell we used electron diffraction in a transmission electron microscope (Figure 2). In this experiment, monolayers of D5TBA were deposited on hydrophilic SiN TEM windows using the LB method. As shown in Figure 2b, the morphology of the islands is the same as on the SiO_2/Si and mica substrates. The diffraction pattern shown in Figure 2c was acquired with a beam size of 100 nm through an individual fingerlike domain (arrow in Figure 2b) and shows

dx.doi.org/10.1021/nl202720y |*Nano Lett.* 2011, 11, 4107–4112

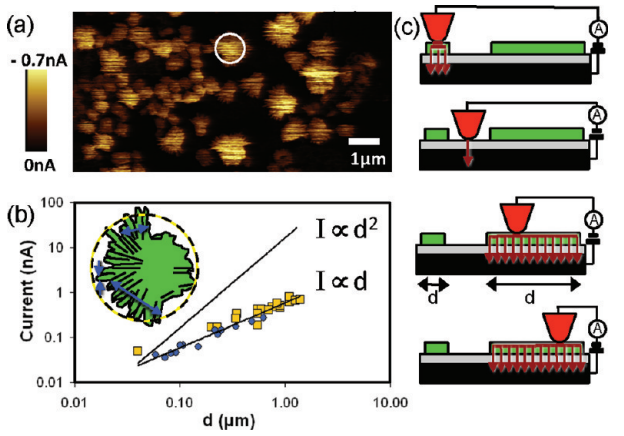

Figure 3. (a) Current-sensing AFM image of D5TBA monolayer islands on a SiO_2/Si-p+ substrate at $V_{sample} = -2.0$ V. (b) Dependence of the current on average island diameter (yellow squares) and on the local width in the *b* lattice direction (blue circles) within islands. Diameter and width are defined in the inset by the yellow circle and the blue arrows. (c) Schematic representation of the AFM-sample contact. On the bare SiO_2/Si substrate current only flows through the SiO_2 in the contact area of the tip. Over the islands the current can flow laterally over a distance *d*, before tunneling through the SiO_2. This gives rise to the island size dependence.

strong (−1,1), (1,1), (2,0), and (2,1) reflections. The conspicuous absence of (1,0) and (0,1) reflections is the result of glide reflection symmetry in the *p2gg* space group, consistent with the Herringbone structure of the unit cell of the D5TBA film (Figure 2a).

We also performed classical molecular dynamics calculations to determine the most stable packing of the D5TBA molecules. We have tested the CFF91 force field,[18] as implemented in the LAMMPS code,[19] as well as the COMPASS force field.[20] We found a better agreement for the COMPASS force field with the experimental results. We have thus rescaled the Lennard-Jones parameter σ by 87% in the CFF91 force field to match the results of the COMPASS force field. This allows us to calculate large systems with the LAMMPS code. Various initial structures and lattice constants were explored. The lowest energy configuration after relaxation is indeed a Herringbone structure (Figure 2a) with the D5TBA molecules inclined to give a film height of 2.7 nm (Figure 1g). The calculated unit cell dimensions are a = 9.5 Å in the [1,0] direction and b = 5.5 Å in the [0,1] direction. The lines in Figure 2a are drawn along directions of close molecular packing, which correspond to the rows resolved in AFM: two equivalent diagonal directions and a third direction parallel to [0,1]. The spacing between parallel rows of 4.8 Å is in agreement with the periodicity measured in the AFM images. The structure measured by electron diffraction is similar to the calculated one with a unit cell that was only slightly different (a = 9.1 ± 0.4 Å, b = 5.9 ± 0.3 Å). Whether this small discrepancy is due to substrate−monolayer interactions is currently under investigation.

We measured the orientation of the long axis in the fingerlike domains relative to the directions of the molecular lattice in both AFM and TEM. AFM images of adjacent domains of D5TBA monolayer on mica revealed that the molecular lattice had a fixed orientation relative to the fingerlike domain short axis with one lattice row direction being always orthogonal to the long axis of the domains. The same comparison was done with TEM from which we conclude that the a = [1,0] and b = [0,1] directions of the unit cell are respectively parallel (as shown in Figure 1e) and orthogonal to the long axis of domains (see Supporting Information Figure S1).

Lateral Charge Transport and Anisotropy. The electrical conduction properties of the D5TBA islands were studied using CAFM. A net load of 15 nN was applied for a reliable electrical contact without noticeable perturbation of the molecules. Much higher loads however do affect the current, an interesting effect that will be described separately in a forthcoming paper. Typical current images are shown in Figures 1d, 3a, and 6a,b. The current level at each pixel of the CAFM current image is the combined result of (1) injection of charge carriers from the tip (substrate) into the monolayer island, (2) transport through the monolayer island, and (3) ejection from the monolayer island into the substrate (tip). The first observation is that for negative sample bias the current is higher on the islands than on the bare SiO_2. This seems counterintuitive: by adding material and increasing the separation between the metallic tip and the substrate by 2.5 nm, the resistance of the junction decreases. In principle, the addition of an organic layer in the junction can increase the tip−sample current by modifying the potential drop in the junction.[21] However, here we demonstrate that the higher current level on the islands is due to lateral conduction across molecules, which increases the effective electrical contact area.

Current images, as those in Figures 3a and 6a, show that at negative sample voltage the current level is significantly higher on the larger islands. Figure 3b shows a log−log plot of the average current for each island as a function of the island size at V_{sample} = −2 V. The current increases linearly with island size up to several micrometers in the largest islands. The lattice periodic structure, thickness of the monolayer, tip−sample contact potential difference (CPD, not shown here), tip load, and the thickness of the SiO_2 are the same for all island sizes, although they may vary locally within an island. Therefore we do not expect that the barriers for injection and ejection of charge carriers in and out of the islands vary with island size. Instead, we propose that the island size dependence of the current at negative sample voltage is the result of charge carrier transport laterally through the monolayer (Figure 3c).

Lateral transport in SPM junctions containing nanometer-size clusters of molecules was first demonstrated by STM measurements of the apparent height as a function of cluster size.[22−24] CAFM provides a more direct method to determine conductivity properties, since the tip−sample distance is controlled independently of the transport current.[25,26] Lateral conduction in a molecular film can become significant if the barrier for carrier transport from molecule to molecule is small compared to the barrier between molecule and substrate. This can be illustrated by a resistor network (see Figure 4c), where N + 1 parallel resistors represent the intermolecule resistances ($R_{mol\text{-}mol}$). Each of the molecules is connected to the substrate by a series resistance ($R_{mol\text{-}sub}$). This leads to a reduction of the total resistance of the junction for the 1D case as $1/R = (1/R_{mol-sub}) + \Sigma_{n=1}^{N}(2/R_{mol-sub} + nR_{mol-mol})$.[22−24] From this it is easy to see that it is thanks to the thin insulating SiO_2 layer that the lateral intermolecular charge transport can be clearly observed in our measurements, that is, $R_{mol\text{-}sub}$ is large compared to $R_{mol\text{-}mol}$. On a substrate without oxide barrier, for example, Au, the vertical transport through the D5TBA molecules is dominant. We should emphasize that an ohmic resistor model does not realistically represent the true transport properties of the molecules and

dx.doi.org/10.1021/nl202720y |*Nano Lett.* 2011, 11, 4107–4112

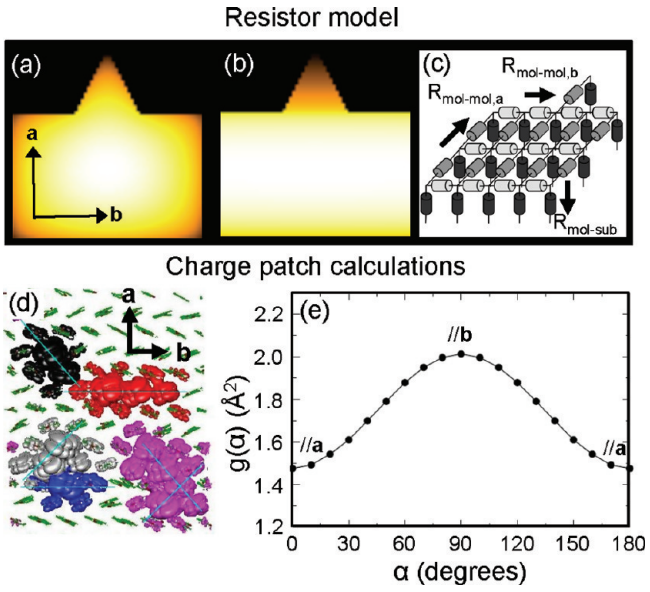

Figure 4. Conduction anisotropy in resistor model and charge patch calculations. (a,b) Calculated current images for a simplified island geometry consisting of a square main body and a fingerlike protrusion using a resistor network. (a) isotropic conduction model, where $R_{mol-mol,a} = R_{mol-mol,b}$. (b) Anisotropic conduction model where $R_{mol-mol,a} > R_{mol-mol,b}$. (c) Resistor network consisting of resistors $R_{mol-mol,a}$ and $R_{mol-mol,b}$ representing the contact resistance between molecules in the a and b directions, and $R_{mol-sub}$ representing the molecule−substrate contact resistance (for clarity only a small network is shown). (d) Top five hole wave functions corresponding to a snapshot in a room temperature molecular dynamics simulation of the 7 × 7 cell Herringbone structure. The globular shapes are isosurfaces enclosing regions with 98% probability of finding the hole inside. The energies of the five levels are 2.787 (blue), 2.758 (red), 2.746 (pink), 2.738 (black), 2.735 eV (gray). (e) Plot of g (proportional to carrier mobility) as a function of the angle α in the unit cell, with 90° corresponding to the b = [0,1] direction.

the tunneling barriers of our tip−molecular island−substrate junctions.

The graph in Figure 3b shows that the current scales linearly rather than quadratically with island diameter. This demonstrates that the current level is not simply proportional to the island area. It also suggests that the conduction is not isotropic. In order to relate the lateral conduction to the structure of the molecular lattice, we focus on the single-domain, fingerlike protrusions of the islands. We observe that the current level increases from the end of the fingerlike protrusions toward the island main body. The current gradient is not continuous but increases by steps when individual fingerlike domains or clusters of fingers connect (this can be observed in Figures 1d and 6a). To quantify these observations, we determined the dependence of current on local width of the domains in the b = [0,1] direction, that is, in the direction orthogonal to a finger long axis (which points in the a-direction). This direction is indicated by blue arrows in the inset of Figure 3b. The data in Figure 3b (blue dots) show that the current scales linearly with local width, which implies that the current is dominated by conduction pathways in the b = [0,1] direction of the domains. To further evaluate the effect of conduction anisotropy we calculated current images for a simplified island shape for isotropic and anisotropic conduction (Figure 4a,b) using a 2D resistor network model

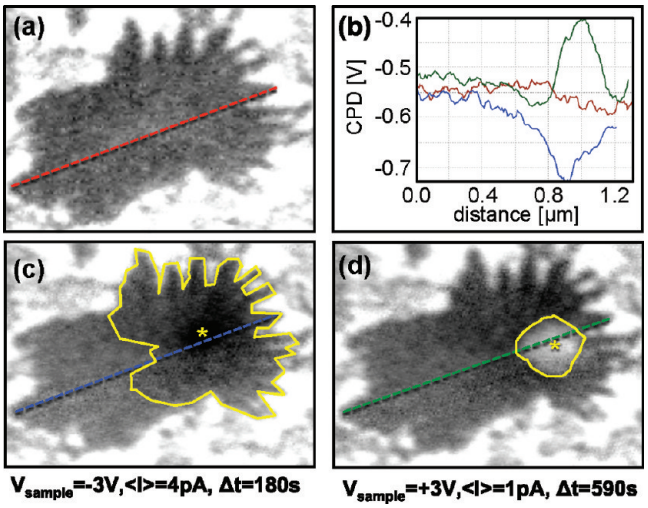

Figure 5. (a,c,d) Kelvin probe microscopy images of the contact potential difference (CPD) between the Pt AFM tip and a D5TBA island (image size = 1.48 × 1.20 μm, NC-AFM parameters: f = 68kHz, Δf = −30 Hz. KPFM sample voltage modulation: frequency f_{KPFM} = 1.2kHz, amplitude A_{KPFM} = 0.05 V). (b) Line profiles of the CPD along the lines in each image (see also Supporting Information). Between (a) and (c) the monolayer was point contacted by the tip at the position marked * at a V_{sample}= −3 V. This resulted in a lowering of the CPD in an area well outside of the tip-island contact. Between (c) and (d) the island was point contacted at V_{sample} = +3 V resulting in an increase in the CPD. Yellow lines mark the boundaries of modified contact potential.

(Figure 4c) (see Supporting Information). For an isotropic resistor network the gradients in the current vary smoothly in all directions, while the anisotropic network reproduces better the characteristic gradients of the protrusions of the experimental CAFM current images. These results suggest that transport occurs preferentially in the b direction, where the thiophene rings of adjacent molecules are parallel to each other.

We used molecular dynamics simulations in a periodic 7 × 7 supercell of D5TBA to gain a molecular level insight on the dependence of conductivity on crystal lattice direction. We calculated the hole wave functions and their overlap at room temperature to estimate the anisotropy of the hole mobility. The calculation was performed using the charge patch method,[27] which has an accuracy similar to that of density functional theory in the local density approximation. A snapshot of the top five hole wave functions is shown in Figure 4d. The hole hopping probability between states k and m is assumed to be proportional to the square of the wave function moduli overlap

$$W_{km} \propto M_{km}^2 = [\int |\psi^{(k)}(\mathbf{r})||\psi^{(m)}(\mathbf{r})|d^3\mathbf{r}]^2$$

where $\psi^{(k)}$ and $\psi^{(m)}$ are the wave functions for the room-temperature structure (not the ideal zero temperature crystal one), which are obtained from snapshots in the molecular dynamics simulation. In recent work,[28] we have shown that such overlap integral approximates very well the full hopping matrix calculated by taking into account the electron−phonon interaction.

The function g, defined as

$$g(\alpha) = \langle[(x_k - x_m)\cos\alpha + (y_k - y_m)\sin\alpha]^2 M_{km}{}^2\rangle$$

is proportional to the diffusion constant and to the carrier mobility by the Einstein relation (see the Supporting Information

dx.doi.org/10.1021/nl202720y |Nano Lett. 2011, 11, 4107–4112

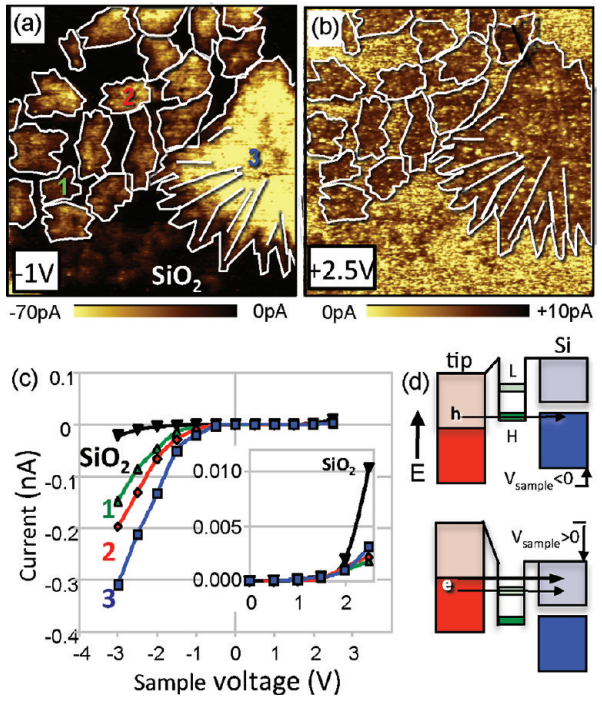

Figure 6. (a) current image at V_{sample} = −1.0 V, (b) current image at V_{sample} = +2.5 V of D5TBA on SiO_2/Si in dry N_2. The outline of the D5TBA islands has been superimposed (see Supporting Information for more details). (c) Current−voltage spectra acquired in the four locations marked in (a). The current is obtained by averaging selected regions of the islands. (d) Schematic energy diagram of charge transport through the tip−molecular island−SiO_2−Si junction. For V_{sample} < 0, holes are injected in the HOMOs of the molecules contacted by the tip. Holes move laterally through the islands across HOMO (H) orbitals of adjacent molecules followed by tunneling through the SiO_2. For V_{sample} > 0 transport results mainly from direct tunneling with a small contribution by lateral transport through the LUMO (L) levels.

for more details). This function quantifies the angular dependence of hole mobility. In Figure 4e, we plot the dependence of g on the direction α. The hole mobility is 30% larger in the b = [0,1] direction than in the a = [1,0] direction, which is in qualitative agreement with our experimental results.

An additional proof for lateral transport is provided by Kelvin probe force microscopy (KPFM), which makes possible to detect local potential distribution due to local dipoles and trapped charges, which we could locally introduce by tip contact at sufficiently high voltages.[29] Figure 5a shows a KPFM image of an island, which appears more negative than the surrounding substrate relative to the tip. The island was subsequently contacted by the tip at the locations marked by a star in (c) and (d), first at V_{sample} = −3 V sample bias (Figure 4c) and later at V_{sample} = +3V (Figure 4d) (see Supporting Information). After contact at V_{sample} = −3 V, positive charges became trapped, while after contact at V_{sample} = +3 V the trapped charges were negative. The amount of trapped charge increased with the duration of the current flow. The measurements however do not provide information on the location of the trapped charges, that is, in the D5TBA island or in the underlying SiO_2. The results however show that they can be found well outside of the CAFM tip contact area of 50 nm, again showing that charge carriers injected into the molecular islands move laterally. We note that the probability of charge trapping was low, so that measurable effects on the current images were only visible after prolonged current flow, much longer than that required to acquire a series of CAFM current images.

Electronic Properties of the D5TBA Monolayer. The electronic properties of the D5TBA islands and of the exposed SiO_2 substrate were studied by current−voltage (I−V) spectroscopy. I−V spectra were obtained by averaging the current over selected regions in images acquired at sample bias between −3 V and +2.5 V in 0.5 V increments (Figure 6a,b). The I−V curves of the Pt−SiO_2−Si junction (acquired on the bare substrate regions) are consistent with tunneling through the oxide with no rectifying effect. The doping level of the silicon is such that it can be considered as a metal. In contrast, I−V curves acquired over the islands show a rectifying behavior. For negative sample voltages the current onset is close to −0.5 V, while for positive voltages the onset is close to +2.0 V. Curves 1, 2, and 3 correspond to the islands marked with the corresponding numbers in Figure 6a. The curves have the same dependence but scale according to their size. The images in Figure 6a,b were acquired at V_{sample} = −1.0 V and +2.5 V, which are 0.5 V below and above the current onsets for negative and positive sample biases (for the complete set see Supporting Information).

The rectifying behavior of a molecular junction[30] can be caused for example by Aviram-Ratner donor−acceptor moieties,[31] asymmetric tunneling barriers,[32−34] Schottky barriers,[35] and pinning of the electronic levels at the molecule/substrate interface.[36] The observed asymmetry of the current shown in Figure 6c is best explained by pinning of the molecular orbitals to the Si substrate Fermi level. Pinning leads to well-defined voltages at which injection of electrons and holes into the lowest unoccupied molecular orbitals (LUMO) and the highest occupied molecular orbitals HOMO respectively becomes efficient (Figure 6d).[37] Pinning to the substrate despite the interposed oxide film can be rationalized first by the strong bond between the butyric acid headgroup and the substrate, as compared to the weak van der Waals interaction between the tip and the methyl end groups of the alkyl chains. Second, the high lateral conductivity of the monolayer effectively enhances the contact area between the thiophene part of the molecular film and the Si substrate.

Unsubstituted oligothiophenes are p-type semiconductors with the HOMO at 4 to 5.5 eV below the vacuum level, which is close to both the Fermi level of Pt on the tip and of the Si.[11] We therefore conclude that the lateral conduction at negative sample voltage is through the HOMO orbitals located approximately 0.5 V below the sample Fermi level (Figure 6e). This agrees with the observation of trapped positive charge (holes, after a conduction measurement at negative sample voltage (Figure 5c). At positive sample bias, the current increases only above +2 V but remains well below the value measured in the tip−SiO_2−Si contacts outside the islands. KPFM demonstrated that at V_{sample} = +3 V at least some electrons were injected in the monolayer islands and that these were transported laterally. Two observations, however, suggest that the lateral electron transport does not contribute substantially to the tip−sample current at positive sample bias; the current image of an island is virtually independent of island size and is not homogeneous, showing strong local spikelike variations (see also Supporting Information). Lateral transport would smear out such local current variations, as observed for negative sample voltages. Therefore only limited lateral transport occurs if an electron is injected into the LUMO. The electron tunnels into the oxide more effectively than hopping to a neighboring molecule. Therefore we ascribe the

dx.doi.org/10.1021/nl202720y |Nano Lett. 2011, 11, 4107–4112

smaller current at positive sample voltages to a much-reduced lateral mobility of the electrons, possibly in combination with a reduced efficiency for electron injection in the LUMO. Mechanisms that could account for a reduced mobility include recombination and scattering by holes in the HOMO or a high density of trap states for electrons.[37]

Conclusions. The structure of decyl-pentathiophene butyric acid (D5TBA) islands on various substrates (SiO_2/Si, mica and SiN TEM supports) has been determined by a combination of AFM topographical and friction imaging, transmission electron microscopy, as well as molecular dynamics calculations. The presence of an insulating oxide film between the D5TBA molecules and the Si substrate electrode made possible the study of lateral conduction, which led to a linear island size dependence of the CAFM tip−substrate current. The electrical properties of the film on SiO_2/Si were investigated by $I-V$ spectroscopy. A strong rectifying behavior was observed with the current being 2 orders of magnitude higher at negative sample voltage, which involves the HOMO orbitals, than at positive voltage. Conduction through the HOMO orbitals increases with island size up to 1.5 μm and shows clear signs of anisotropy with higher conductivity orthogonal to the domain growth direction, which corresponds to the direction where π-orbitals of the thiophene units overlap more strongly. Our study provides a clear link between the molecular level orbital structure, crystallography, and electronic properties of the films.

■ ASSOCIATED CONTENT

Supporting Information. Additional information and figures. This material is available free of charge via the Internet at http://pubs.acs.org.

■ AUTHOR INFORMATION

Corresponding Author

*E-mail: MBSalmeron@lbl.gov.

Present Addresses

[▽]Institute for Molecules and Materials, Radboud University, 6525 AJ Nijmegen,The Netherlands.

[○]Department of Electrical Engineering, Princeton University, Princeton, New Jersey 08544.

[◆]Scientific Computing Laboratory, Institute of Physics Belgrade, University of Belgrade, Pregrevica 118, 11080 Belgrade, Serbia.

■ ACKNOWLEDGMENT

This work was supported by the Office of Science, Office of Basic Energy Sciences, Materials Science and Engineering of the U.S. Department of Energy under Contract No. DE-AC02-05CH11231. V.A. and S.A. are supported by the Molecular Foundry, Lawrence Berkeley National Laboratory. The simulations were performed using the resources of National Energy Research Scientific Computing Center (NERSC).

■ REFERENCES

(1) Forrest, S. R. *Nature* **2004**, *428*, 911–918.

(2) Joachim, C.; Gimzewski, J. K.; Aviram, A. *Nature* **2000**, *408*, 541–548.

(3) Holmlin, R. E.; Haag, R.; Chabinyc, M. L.; Ismagilov, R. F.; Cohen, A. E.; Terfort, A.; Rampi, M. A.; Whitesides, G. M. *J. Am. Chem. Soc.* **2001**, *123*, 5075–5085.

(4) Xu, B. Q.; Tao, N. J. J. *Science* **2003**, *301*, 1221–1223.

(5) Smits, E. C. P.; Mathijssen, S. G. J.; van Hal, P. A.; Setayesh, S.; Geuns, T. C. T.; Mutsaers, K.; Cantatore, E.; Wondergem, H. J.; Werzer, O.; Resel, R.; Kemerink, M.; Kirchmeyer, S.; Muzafarov, A. M.; Ponomarenko, S. A.; de Boer, B.; Blom, P. W. M.; de Leeuw, D. M. *Nature* **2008**, *455*, 956–959.

(6) Dimitrakopoulos, C. D.; Malenfant, P. R. L. *Adv. Mater.* **2002**, *14*, 99.

(7) Yang, H. C.; Shin, T. J.; Ling, M. M.; Cho, K.; Ryu, C. Y.; Bao, Z. N. *J. Am. Chem. Soc.* **2005**, *127*, 11542–11543.

(8) Kelley, T. W.; Granstrom, E. L.; Frisbie, C. D. *Adv. Mater.* **1999**, *11*, 261.

(9) Gershenson, M. E.; Podzorov, V.; Morpurgo, A. F. *Rev. Mod. Phys.* **2006**, *78*, 973–989.

(10) Moser, C. C.; Keske, J. M.; Warncke, K.; Farid, R. S.; Dutton, P. L. *Nature* **1992**, *355*, 796–802.

(11) Murphy, A. R.; Frechet, J. M. J. *Chem. Rev.* **2007**, *107*, 1066–1096.

(12) Coakley, K. M.; McGehee, M. D. *Chem. Mater.* **2004**, *16*, 4533–4542.

(13) Chen, J. Y.; Murphy, A. R.; Esteve, J.; Ogletree, D. F.; Salmeron, M.; Frechet, J. M. J. *Langmuir* **2004**, *20*, 7703–7710.

(14) Ratera, I.; Chen, J.; Murphy, A.; Ogletree, D. F.; Frechet, J. M. J.; Salmeron, M. *Nanotechnology* **2005**, *16*, S235–S239.

(15) Chen, J.; Ratera, I.; Murphy, A.; Ogletree, D. F.; Frechet, J. M. J.; Salmeron, M. *Surf. Sci.* **2006**, *600*, 4008–4012.

(16) Kelley, T. W.; Frisbie, C. D. *J. Phys. Chem. B* **2001**, *105*, 4538–4540.

(17) Salmeron, M. *Tribol. Lett.* **2001**, *10*, 69–79.

(18) Hwang, M. J.; Stockfisch, T. P.; Hagler, A. T. *J. Am. Chem. Soc.* **1994**, *116*, 2515–2525.

(19) Plimpton, S. *J. Comput. Phys.* **1995**, *117*, 1–10.

(20) Sun, H. *J. Phys. Chem. B* **1998**, *102*, 7338–7364.

(21) Yan, H. J.; McCreery, R. L. *ACS Appl. Mater. Interfaces* **2009**, *1*, 443–451.

(22) Ishida, T.; Mizutani, W.; Akiba, U.; Umemura, K.; Inoue, A.; Choi, N.; Fujihira, M.; Tokumoto, H. *J. Phys. Chem. B* **1999**, *103*, 1686–1690.

(23) Yokota, Y.; Fukui, K.; Enoki, T.; Hara, M. *J. Am. Chem. Soc.* **2007**, *129*, 6571–6575.

(24) Kafer, D.; Bashir, A.; Dou, X.; Witte, G.; Mullen, K.; Woll, C. *Adv. Mater.* **2010**, *22*, 384–+.

(25) Fang, L.; Park, J. Y.; Ma, H.; Jen, A. K. Y.; Salmeron, M. *Langmuir* **2007**, *23*, 11522–11525.

(26) Qi, Y. B.; Liu, X. S.; Hendriksen, B. L. M.; Navarro, V.; Park, J. Y.; Ratera, I.; Klopp, J. M.; Edder, C.; Himpsel, F. J.; Frechet, J. M. J.; Haller, E. E.; Salmeron, M. *Langmuir* **2010**, *26*, 16522–16528.

(27) Vukmirovic, N.; Wang, L. W. *J. Phys. Chem. B* **2009**, *113*, 409–415.

(28) Vukmirovic, N.; Wang, L. W. *Appl. Phys. Lett.* **2010**, *97*, 043305.

(29) Heim, T.; Lmimouni, K.; Vuillaume, D. *Nano Lett.* **2004**, *4*, 2145–2150.

(30) Metzger, R. M. *Chem. Rev.* **2003**, *103*, 3803–3834.

(31) Aviram, A.; Ratner, M. A. *Chem. Phys. Lett.* **1974**, *29*, 277–283.

(32) Datta, S.; Tian, W. D.; Hong, S. H.; Reifenberger, R.; Henderson, J. I.; Kubiak, C. P. *Phys. Rev. Lett.* **1997**, *79*, 2530–2533.

(33) Kornilovitch, P. E.; Bratkovsky, A. M.; Williams, R. S. *Phys. Rev. B* **2002**, *66*, 165436.

(34) Krzeminski, C.; Delerue, C.; Allan, G.; Vuillaume, D.; Metzger, R. M. *Phys. Rev. B* **2001**, *64*, 085405.

(35) Liu, Y. Q.; Xu, Y.; Zhu, D. B. *Synth. Met.* **1997**, *90*, 143–146.

(36) Lenfant, S.; Guerin, D.; Van, F. T.; Chevrot, C.; Palacin, S.; Bourgoin, J. P.; Bouloussa, O.; Rondelez, F.; Vuillaume, D. *J. Phys. Chem. B* **2006**, *110*, 13947–13958.

(37) Chua, L. L.; Zaumseil, J.; Chang, J. F.; Ou, E. C. W.; Ho, P. K. H.; Sirringhaus, H.; Friend, R. H. *Nature* **2005**, *434*, 194–199.